A database for MR-based electrical properties tomography with in silico brain data—ADEPT

T. G. Meerbothe[1,2] | **E. F. Meliado[1,2]** | **P. R. S. Stijnman[1,2]** | **C. A. T. van den Berg[1,2]** | **S. Mandija[1,2]**

[1]Department of Radiotherapy, Division of Imaging and Oncology, University Medical Center Utrecht, Utrecht, The Netherlands

[2]Computational Imaging Group for MR Therapy and Diagnostics, Center for Image Sciences, University Medical Center Utrecht, Utrecht, The Netherlands

Correspondence
T. G. Meerbothe, Department of Radiotherapy, Division of Imaging and Oncology, University Medical Center Utrecht, Utrecht, The Netherlands.
Email: t.g.meerbothe@umcutrecht.nl

Funding information
Netherlands Organisation for Scientific Research (NWO), Grant/Award Number: 18078

Abstract

Purpose: Several reconstruction methods for MR-based electrical properties tomography (EPT) have been developed. However, the lack of common data makes it difficult to objectively compare their performances. This is, however, a necessary precursor for standardizing and introducing this technique in the clinical setting. To enable objective comparison of the performances of reconstruction methods and provide common data for their training and testing, we created ADEPT, a database of simulated data for brain MR-EPT reconstructions.

Methods: ADEPT is a database containing in silico data for brain EPT reconstructions. This database was created from 25 different brain models, with and without tumors. Rigid geometric augmentations were applied, and different electrical properties were assigned to white matter, gray matter, CSF, and tumors to generate 120 different brain models. These models were used as input for finite-difference time-domain simulations in *Sim4Life*, used to compute the electromagnetic fields needed for MR-EPT reconstructions.

Results: Electromagnetic fields from 84 healthy and 36 tumor brain models were simulated. The simulated fields relevant for MR-EPT reconstructions (transmit and receive RF fields and transceive phase) and their ground-truth electrical properties are made publicly available through ADEPT. Additionally, nonattainable fields such as the total magnetic field and the electric field are available upon request.

Conclusion: ADEPT will serve as reference database for objective comparisons of reconstruction methods and will be a first step toward standardization of MR-EPT reconstructions. Furthermore, it provides a large amount of data that can be exploited to train data-driven methods. It can be accessed from https://doi.org/10.34894/V0HBJ8.

KEYWORDS
brain models, conductivity, database, electrical properties tomography, standardization

1 | INTRODUCTION

MR-based electrical properties tomography (EPT) is a technique in which electrical properties (EPs, conductivity σ and relative permittivity ϵ_r) are reconstructed from noninvasive MR measurements. Knowledge of EPs is essential for accurate, personalized specific absorption rate calculations in RF safety applications.[1,2] Furthermore, because at RF frequencies EPs are dependent on the underlying tissue composition, they can be a biomarker for use in clinical applications, as outlined in different studies.[3–6] For these reasons, increasingly more research has been devoted on the development of reconstruction methods for EPT, resulting in numerous different methods.[7]

Tissue EPs are imprinted in the magnetic fields as described by Maxwell's equations. The aim of EPT is to derive these EPs from the measured transmit and/or receive RF field. EPT reconstruction methods are generally divided into two classes: direct and inverse approaches. In direct approaches, the EPs are calculated from the measured B_1^+ field directly, and the methods often rely on the calculation of derivatives of the B_1^+ field. The most common direct approach is Helmholtz EPT, which relates the Laplacian of the B_1^+ field to the EPs.[1,8] However, direct approaches like Helmholtz EPT, operating on measured noisy data, generally suffer from issues at boundaries between tissues and noise amplification. This is a result of the discrete spatial derivatives and assumptions in the derived equations.[9,10] Several methods have been developed to reduce these problems. For example, convection reaction EPT solves for the equations without the assumption that the EPs are piecewise constant,[11] whereas other methods suppress noise via fitting approaches using magnitude-based kernels and image-based postprocessing filters.[12,13] On the other hand, inverse methods such as Contrast Source Inversion[14] and Global Maxwell Tomography[15] use EPs to estimate resulting fields, and rely on minimization of a cost function to reconstruct EPs. They generally show promising results for reducing noise and boundary effects but suffer from a high computational load and convexity issues.

More recently, data-driven methods have been presented for EPT reconstructions that have been found to successfully reduce the noise amplification and boundary errors. Such methods use either deep learning strategies for end-to-end predictions[16,17] or provide initial estimates for iterative reconstruction schemes.[18]

An important downside of data-driven reconstruction methods is that training requires large datasets, which are computationally expensive to create. Although the presented results are promising despite the relatively little amount of training data used, a larger amount of more diverse data are necessary to improve generalization to unforeseen cases.

A key issue for comparing the performance of the presented reconstruction methods in literature is the lack of common data, limiting objective comparison. In fact, current reconstruction methods are presented and tested on custom data, which make objective comparison impossible, but this is an essential step toward standardization and clinical introduction of EPT in the future.

To address these issues, we developed "A Database for MR Electrical Properties Tomography" (ADEPT) containing simulated data for EPT reconstructions in the brain region. The key goal of ADEPT is to provide a large amount of simulated data for EPT reconstruction. This will enable (1) objective benchmarking of reconstruction methods on common data for future standardization of EPT methods and (2) a reduction of the computational burden for the creation of large datasets to train deep learning–based EPT methods. We aim to provide the data in ADEPT according to the Findable, Accessible, Interoperable and Reusable (FAIR) paradigm.[19]

2 | METHODS

2.1 | Creation of brain models

ADEPT consists of in silico data for EPT reconstruction in the brain region. In total, 120 brain models were generated: 84 healthy brain models and 36 pathological brain models with realistic tumor inclusions. All brain models consisted of white matter (WM), gray matter (GM), CSF, and tumor regions (if applicable). Other types of tissues present in the brain, such as blood vessels and dura mater, were generalized into WM, GM or CSF tissue, which is a realistic approximation.[20]

Seven anatomically different healthy brain models were selected from the BrainWeb database, an online database with simulated 3D brains.[21] The BrainWeb models were already segmented into 12 different discrete tissues, including WM, GM, and CSF. These seven models were manually modified using *Slicer 3D*.[22] In particular, the 12 presegmented tissues were combined into WM, GM, and CSF. Moreover, the tissues were smoothed, and the CSF layer was enlarged by 3 mm to preserve the structure when a coarser voxelization was used in the electromagnetic simulations (see Section 2.3).

Eighteen anatomically different brain models with tumor inclusions were also selected from the BraTS data set,[23] consisting of T_1-weighted images of brain tumor patients and segmentations of the different pathological regions. In this work, we used the same labels as proposed in the BraTS data set description: edema, active tumor
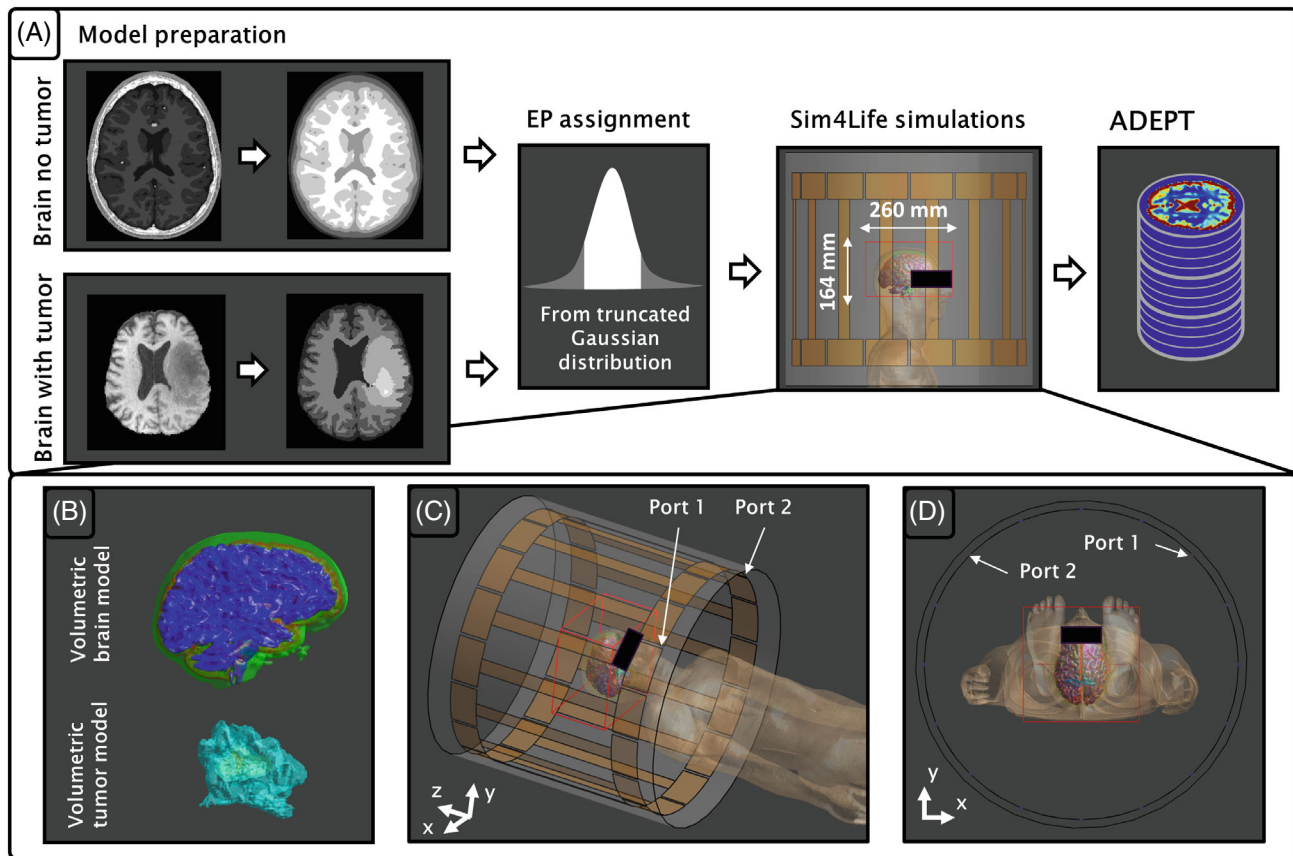
FIGURE 1 Overview of the data creation pipeline for ADEPT ("A Database for MR Electrical Properties Tomography") and simulation setup in *Sim4Life*. (A) Pipeline to create in silico data for brain electrical properties tomography (EPT) reconstructions. (B) Example of the resulting volumetric models that are imported in *Sim4Life*. (C) Simulation setup in *Sim4Life*, with the brain in the center of the coil. Output fields within the red box are extracted. (D) Top view of simulation setup.

(AT), which shows hyperintensities in contrast-enhanced T_1 images, and nonenhancing tumor (NET), which typically shows hypo-intensities in contrast-enhanced T_1 images.[24] Starting from the T_1-weighted images, the WM, GM, and CSF were segmented using *SPM12* (Functional Imaging Laboratory, University College London, UK). For each brain model, the presegmented pathological tissues were then overlaid to the segmented healthy tissues.

With this procedure, a total of 25 anatomically different brain models were obtained as visualized in the first part of Figure 1A. To increase the amount of data attainable from these models, different augmentations were done (see Section 2.2).

As a final step, both the healthy brain models and the models including a tumor were converted into volumetric surface models that were imported into the electromagnetic simulation software *Sim4Life* (Zurich MedTech, Zurich, Switzerland) (see Section 2.3). Here, the brain models were inserted into a general body model (Duke from the virtual population) to achieve realistic coil loading for the simulations, thus replacing Duke's original

brain.[25] For this, affine transformations (translations, rotations, and scaling) were applied to fit the custom brain models to the brain of Duke, and higher priority was assigned to these custom brains during voxelization.

2.2 | Data augmentation and EP assignment

To augment the 25 initial brain models, several augmentations including geometric augmentations (i.e., rotations and translations) of the whole-body model, and EP augmentations by assigning different EPs values to the segmented brain tissues, were performed.

Each healthy brain model was augmented 12 times, first using three different geometric augmentations, and then, for each geometrically augmented model, four different combinations of tissue EPs were applied. Instead, for the tumor models, only EP-based augmentations were performed, in which two different sets of conductivity values were assigned to the pathological tissues, whereas EPs in WM, GM, and CSF were kept the same.

In particular, geometric augmentations include translations (± 1 cm displacements in either x, y, or z direction) and rotations ($\pm 5º$ rotations around the x, y, or z axis). For each model, a different combination of one or two translations and/or rotations were applied. All geometric augmentations were applied to both the body model and the custom brain.

For the assignment of different EPs, random combinations of EPs were drawn from truncated Gaussian distributions with assigned mean and SD. Specifically, for the healthy brain models, mean conductivity and permittivity values were set according to literature values: 0.34, 0.59, and 2.14 S/m for conductivity and 52.5, 73.5, and 84 for permittivity for WM, GM, and CSF, respectively.[26,27] The corresponding SD was 0.08 s/m for the conductivity and 1.5 for the permittivity.

For the brain models with tumor inclusions, these reported mean conductivity and permittivity values were used for WM, GM, and CSF. Brain tumor conductivity has been shown to have higher values than normal tissue and to contain large variations both within tumor substructures and between tumor types.[3,28] To reflect these variations, tumor conductivity values were also drawn from truncated Gaussian distributions with mean values of 0.70, 0.90, and 1.20 S/m for edema, NET and AT, respectively, all with a SD of 0.15 S/m.[3,6,28] For permittivity, these values are not readily available, but the expected permittivity in lesions should be higher than healthy tissue due to changes in water content.[29] Because of limited in vivo MR-EPT studies on tissue permittivity in lesions at 128 MHz, we assigned constant indicative values of 60, 80 and 70, respectively, for edema, NET, and AT.

Truncation was done to prevent overlap of EP values for the healthy and tumor tissues and limit large EP value outliers. This led to EP ranges as described in Figure 2C.

2.3 | Simulations

All simulations were performed in *Sim4Life* on an approximate 1-mm isotropic grid size as retrieved from the voxelization in *Sim4Life*. Little variations in the grid size were present, as certain parts of the coil needed to be voxelized on a finer grid. This was corrected by resampling in postprocessing (Section 2.4). Simulations were done using a 3T birdcage coil with ports at 45º, similar to the clinical coil, with the same geometry as previous studies.[30] A rectangular area centered around the coil isocenter was defined as the export region for all fields. This region encompassed the brain and had dimensions of 260 mm in the x and y direction and 164 mm in the z direction. Simulations were executed in both quadrature (QA) mode for transmit and antiquadrature (AQ) mode for receive to

allow computation of the transceive phase, as previously reported in literature.[16]

The following fields were simulated and exported, after normalization to 1 W input power:

- B_1^+ (QA and AQ) transmit magnetic field (B_1^+ [T])
- B_1^- (QA and AQ) receive magnetic field (B_1^- [T])
- Magnetic flux density vector (**B** [T])
- Magnetic field intensity vector (**H** [A/m])
- Electric field vector (**E** [V/m])
- Electric displacement field vector (**D** [C/m^2]), computed as $\boldsymbol{D} = \varepsilon_r \boldsymbol{E} \varepsilon_0$
- Current density vector (**J** [A/m^2]), computed as $\boldsymbol{J} = \sigma \boldsymbol{E}$
- Voxelization grid information

Here, following the conventions of *Sim4Life*, the circularly polarized fields (B_1^+ and B_1^-) are defined in a right-handed coordinate system:

$$B_1^+ = \frac{1}{2}\left(B_{1,x} + iB_{1,y}\right) \tag{1}$$

$$B_1^- = \frac{1}{2}\left(B_{1,x} - iB_{1,y}\right)^* \tag{2}$$

where the asterisk denotes the conjugate. The complete data creation pipeline is visualized in Figure 1A. An overview of the simulation setup in *Sim4Life* can be seen in Figure 1B–D.

2.4 | Postprocessing

From the exported fields, the transmit phase (ϕ^+ [rad]) and B_1^+ magnitude ($|B_1^+|$ [T]) were taken directly from B_1^+ data of the simulation in QA mode, whereas the transceive phase ($\phi^\pm$ [rad]) was calculated using the known relation as follows[31]:

$$\varphi^\pm = \varphi^+ + \varphi^- \tag{3}$$

where ϕ^- was retrieved as the receive phase from B_1^- in AQ mode.

By using the voxelization grid information, all data were interpolated in 3D to ensure an isotropic 1-mm grid. For ground-truth conductivity and permittivity, this was done using nearest-neighbor interpolation to prevent partial volume effects that were not present in the simulated, voxelized brain models. For all other fields, a linear interpolation was done. Next, brain-tissue masks and tissue segmentations were created based on the ground-truth conductivity and permittivity values. Finally, the data were masked to include only WM, GM, CSF, and tumor.

2.5 | Database evaluation

To demonstrate the validity of the simulated electromagnetic fields, EPT reconstructions were done using the simulated complex B_1^+ field and compared with the input EPs. For this, 3D Helmholtz reconstructions with a 3-point kernel were done as follows[7]:

$$\sigma = \frac{1}{\mu_0 \omega} \text{Im} \left\{ \frac{\nabla^2 B_1^+}{B_1^+} \right\} \qquad (4)$$

$$\epsilon_r = \frac{-1}{\epsilon_0 \mu_0 \omega^2} \text{Re} \left\{ \frac{\nabla^2 B_1^+}{B_1^+} \right\} \qquad (5)$$

where the simulated transmit phase was used to avoid errors from the transceive phase assumption. Furthermore, μ_0 is the vacuum permeability and ω is the Larmor frequency. Evaluation was done in the WM, GM, and CSF after erosion of three voxels, as previously done in literature.[32]

3 | RESULTS

Using the created simulation pipeline, in total 120 brain models were simulated (7×12 healthy models and 2×18 models with tumor inclusions).

Simulations for a single model (QA and AQ) took approximately 4 h on an NVIDIA GeForce RTX 3090 Ti GPU, resulting in a total simulation time of approximately 480 h. Per model, corresponding output was saved in a single.mat file with an approximate size of 300 MB, for a total database size of 36 GB.

In Figure 2A,B examples of the ground-truth conductivity and permittivity of different simulated brain models are shown for the center slice of the FOV (9 healthy and 4 including tumor). From these examples, clear variation in brain structure and ground-truth EPs can be observed.

As described in Section 2, the simulated data included all fields for EPT reconstruction: B_1^+ magnitude and transceive phase. Apart from these fields, other electromagnetic fields, tissue segmentations, and ground-truth values were simulated. An overview of the output data can be seen in Figure 3. All these data are made available through ADEPT.

Figure 4 demonstrates the validity of the simulated electromagnetic fields. In Part A, conductivity and permittivity reconstructions are shown on two models with the same anatomy, but different EPs (top row). The middle row shows these reconstructions after erosion of three voxels at tissue boundaries. The bottom row shows the percentage error maps with respect to the ground truth (simulation input). Part B shows the distribution of the mean percentage error for EPs reconstructions after three voxel erosions over all models in the database. The error is below 0.4% and 0.7% for conductivity and permittivity, respectively, demonstrating that the simulated fields are consistent with the input EPs.

ADEPT has been made available online using Dataverse,[33] in a structure that is summarized in Figure 5. The data can be found at https://doi.org/10.34894/V0HBJ8. Here, B, D, E, H, and J fields can only be provided upon request due to online storage limitations. Apart from the data, metadata are also provided, describing all anatomical transformations and ground-truth EPs for each simulated model. With this, ADEPT overall follows the FAIR principles.[19]

Furthermore, scripts for noise generation are included to enable EP reconstructions on noisy data. Additionally, because some reconstructions use T_1-weighted and/or T_2-weighted images, scripts to generate synthetic T_1-weighting and T_2-weighting from the tissue-segmentation masks are also provided.[34]

4 | DISCUSSION

ADEPT is the first database for MR-EPT reconstructions with openly available simulated data. In this first implementation, ADEPT contains simulated data for brain EPT reconstructions. A total of 120 different brain models were used as input for electromagnetic simulations, of which 84 were healthy and 36 had tumor inclusions. All simulated data and ground-truth EPs are made available online.

ADEPT enables objective comparison of EPT reconstruction methods on common data, hence allowing a better understanding of their strengths and weaknesses. This, in combination with the first EPT reconstruction challenge, will pave the way to standardization and clinical introduction of EPT.[35]

Furthermore, the large amount of simulated data available through ADEPT significantly alleviates the computational burden for the creation of a large dataset to train data-driven reconstruction methods. As a result, it becomes easier and less time consuming to develop data-driven EPT reconstruction methods.

An additional advantage of ADEPT is that, by providing ready-to-use data, it will lower the threshold for new research groups to start with research on MR-EPT. This works in great synergy with the availability of reconstruction algorithms such as the ones provided in *EPTlib*.[36]

The simulated fields are consistent with the input EPs. A negligible interpolation artifact is observed in the middle of the anterior–posterior and left–right directions because of tight voxelization before regridding (below 1 mm). Nonetheless, the mean percentage errors are lower
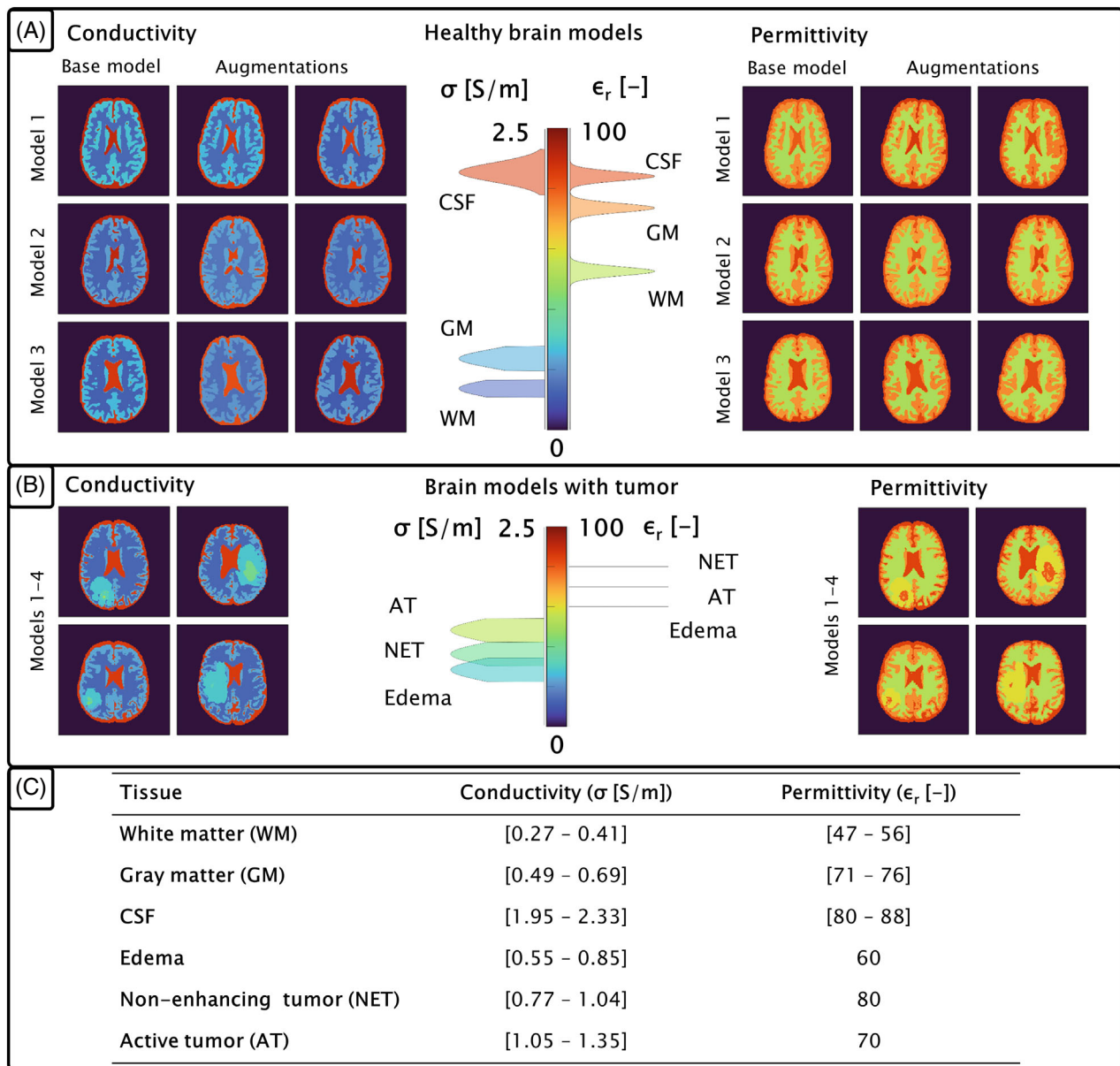
FIGURE 2 Examples of augmented brain models without (A) and with (B) tumor inclusion are shown for both conductivity and permittivity. For the brain models without tumor inclusion, the examples include a base model in the first column and different augmentations (geometric and electrical properties [EP] values) in the second and third columns. The distribution in the color bar in the middle shows the range of values of each tissue. The table in (C) shows the ranges of the conductivity and permittivity values for the different tissues in the simulated brain models. AT, active tumor; GM, gray matter; NET, nonenhancing tumor; WM, white matter.

Tissue	Conductivity (σ [S/m])	Permittivity (ϵ_r [–])
White matter (WM)	[0.27 – 0.41]	[47 – 56]
Gray matter (GM)	[0.49 – 0.69]	[71 – 76]
CSF	[1.95 – 2.33]	[80 – 88]
Edema	[0.55 – 0.85]	60
Non–enhancing tumor (NET)	[0.77 – 1.04]	80
Active tumor (AT)	[1.05 – 1.35]	70

than 0.4% and 0.7%, respectively, for conductivity and permittivity for all tissues after erosion of tissue boundaries, which demonstrates the consistency between the input EPs and the simulated fields. Additionally, for a cylindrical phantom, the simulated fields (B_1^+ magnitude and transceive phase) are comparable to measured fields, and conductivity reconstructions from simulations match conductivity reconstructions from measurements, as shown in the Supporting Information, Data S1, and Figure S1.

However, this first implementation of ADEPT is far from exhaustive, as it only includes 3T simulations using

realistic human brain models. Of course, more data are needed to reach a comprehensive database, such as simulated data from different anatomical regions, simulated data at different field strengths, and measured data on calibrated phantoms and in vivo. We intend to further extend ADEPT by including measured data in the future. In light of a community-shared effort, other curated datasets available in different research centers can also be incorporated. Furthermore, all data from the EPT reconstruction challenge will also be shared in ADEPT. Finally, when other pathological models (e.g., stroke, multiple sclerosis) and
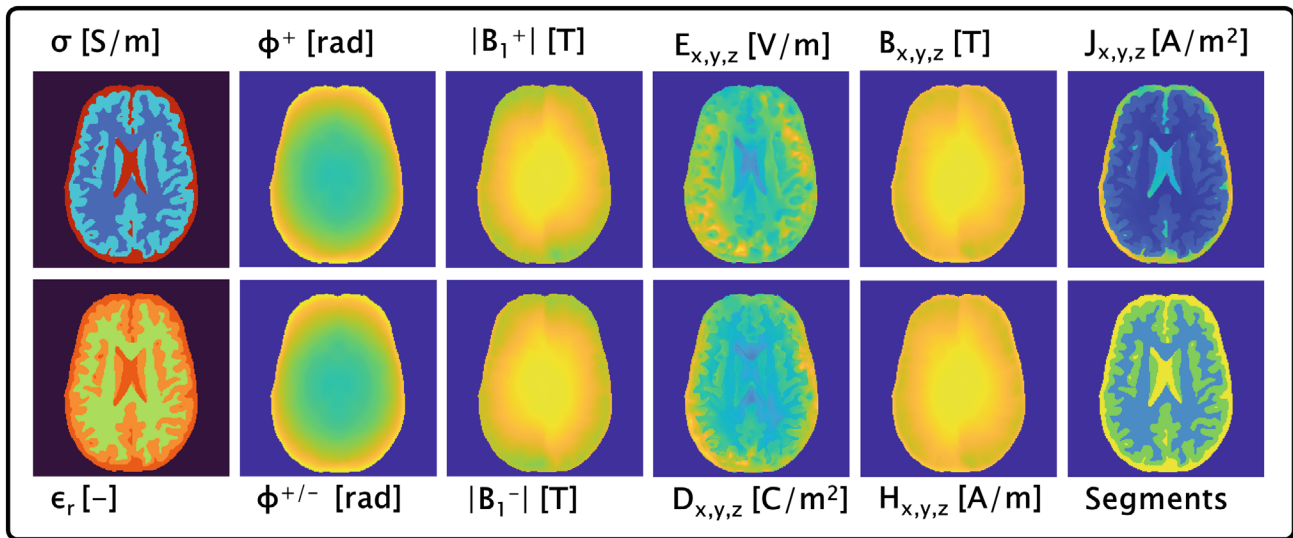
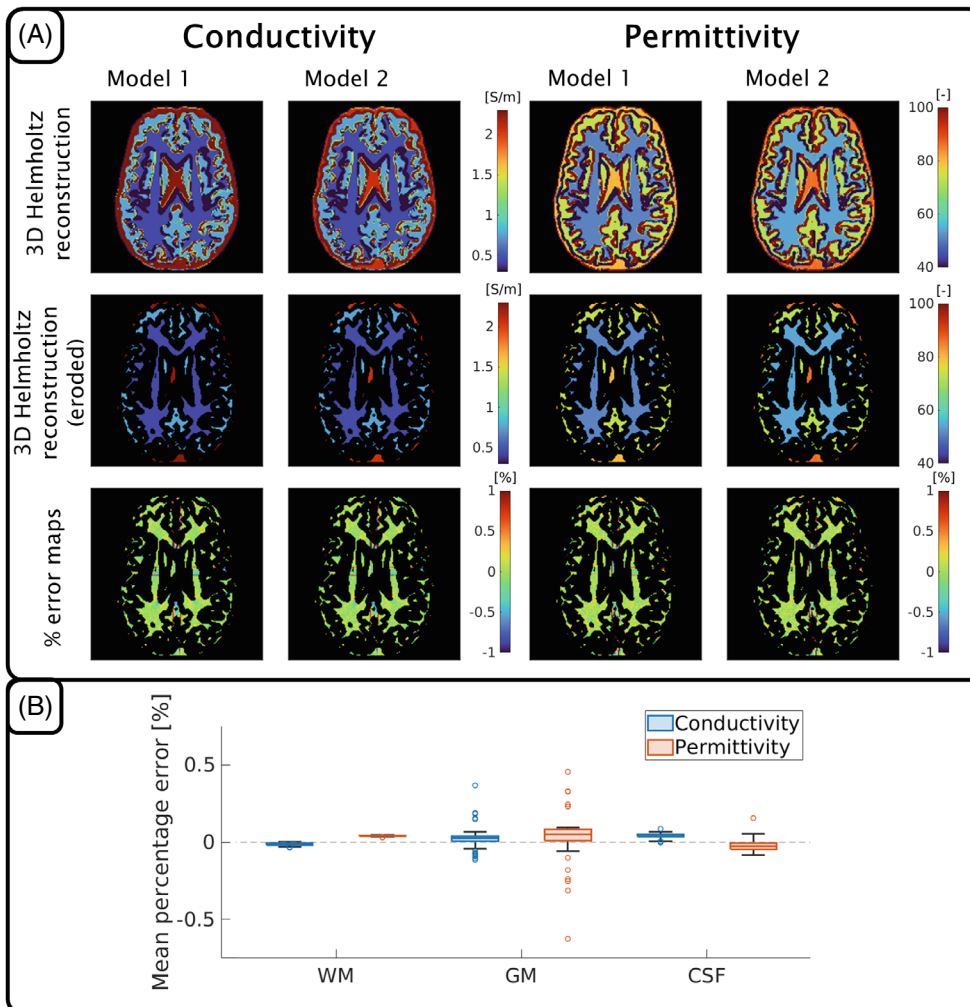**FIGURE 3** Overview of all the simulated output.

FIGURE 4 Validation of the database. (A) Helmholtz electrical properties tomography (EPT) reconstructions for two different models with the same geometry but different electrical properties (EPs) without erosion of tissue boundaries (top row) and with three-voxel erosion of boundaries (second row). The third row shows the percentage error maps with respect to the ground-truth EPs. (B) A boxplot with the mean percent error among all models is shown for white matter (WM), gray matter (GM), and CSF.
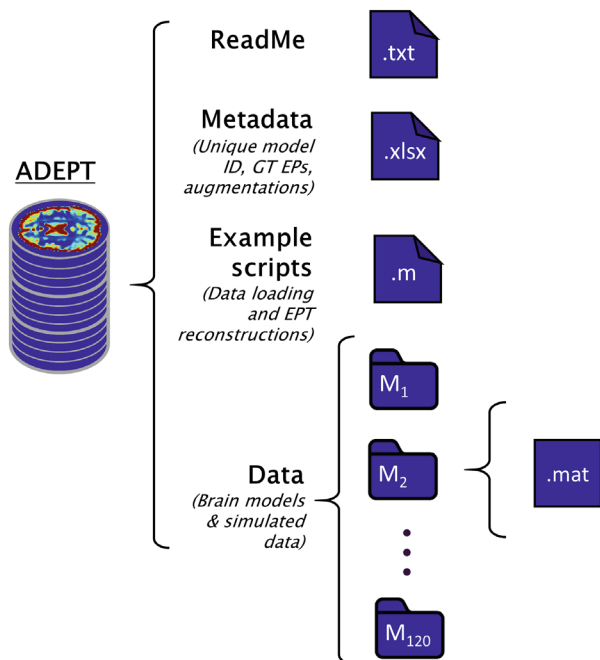
FIGURE 5 Overview of the database structure of ADEPT ("A Database for MR Electrical Properties Tomography"). Apart from the simulated brain models, the database contains metadata and exemplary scripts to generate noise and T_1-weighted, T_2-weighted data. All the data are contained in separate .mat files. EP, electrical properties; EPT, electrical properties tomography.

corresponding EP values are available, the presented pipeline can be used to create new simulated data.

For the current implementation of ADEPT, few design choices have been made to keep simulation time and database size manageable. First, to limit the model complexity, the brain models are a simplification of an actual brain, as they include only WM, GM, CSF, and tumor structures when applicable with piece-wise constant EPs. Furthermore, partial volume effects were not included in the models. Next, the use of a general head/body model as envelope to fit the custom brain models results in the same head/body size in every simulation. Other head/body models may be used in the future to increase variation in head size and tissues outside the brain (eg, fat, muscle). Finally, a choice for 1-mm isotropic resolution was made as the lower bound from presented literature data.[12]

5 | CONCLUSIONS

With this work we present ADEPT, a FAIR database with in silico data using realistic brain models for EPT reconstructions. The database can be used for comparisons of reconstruction methods on common data and, given the large variability in the simulated data, it can help facilitate the development of data-driven methods that need large amounts of data for training. It also lowers the threshold for a new research group to start with EPT.

CONFLICT OF INTEREST STATEMENT
Nothing to report.

DATA AVAILABILITY STATEMENT
The data is available online from: https://doi.org/10.34894/V0HBJ8.

ORCID
T. G. Meerbothe https://orcid.org/0009-0009-5736-1038
P. R. S. Stijnman https://orcid.org/0000-0001-8277-1420
S. Mandija https://orcid.org/0000-0002-4612-5509

REFERENCES
1. Katscher U, Voigt T, Findeklee C, Vernickel P, Nehrke K, Doessel O. Determination of electric conductivity and local SAR via B1 mapping. *IEEE Trans Med Imaging.* 2009;28:1365-1374. doi:10.1109/TMI.2009.2015757
2. Brink WM, Yousefi S, Bhatnagar P, Remis RF, Staring M, Webb AG. Personalized local SAR prediction for parallel transmit neuroimaging at 7T from a single T1-weighted dataset. *Magn Reson Med.* 2022;88:464-475. doi:10.1002/mrm.29215
3. Tha KK, Katscher U, Yamaguchi S, et al. Noninvasive electrical conductivity measurement by MRI: a test of its validity and the electrical conductivity characteristics of glioma. *Eur Radiol.* 2018;28:348-355. doi:10.1007/s00330-017-4942-5
4. Ko IO, Choi BK, Katoch N, et al. In vivo conductivity imaging of tissue response after radiation therapy. In: *Proceedings of the 26th Annual Meeting of ISMRM*, Paris, France. 2018 Abstract #547.
5. Mori N, Tsuchiya K, Sheth D, et al. Diagnostic value of electric properties tomography (EPT) for differentiating benign from malignant breast lesions: comparison with standard dynamic contrast-enhanced MRI. *Eur Radiol.* 2019;29:1778-1786. doi:10.1007/s00330-018-5708-4
6. Shin J, Kim MJ, Lee J, et al. Initial study on in vivo conductivity mapping of breast cancer using MRI. *J Magn Reson Imaging.* 2015;42:371-378. doi:10.1002/jmri.24803
7. Leijsen R, Brink W, van den Berg CAT, Webb A, Remis R. Electrical properties tomography: a methodological review. *Diagnostics.* 2021;11:176. doi:10.3390/diagnostics11020176
8. Voigt T, Katscher U, Doessel O. Quantitative conductivity and permittivity imaging of the human brain using electric properties tomography. *Magn Reson Med.* 2011;66:456-466. doi:10.1002/mrm.22832

9. Mandija S, Sbrizzi A, Katscher U, Luijten PR, van den Berg CAT. Error analysis of helmholtz-based MR-electrical properties tomography. *Magn Reson Med.* 2018;80:90-100. doi:10.1002/mrm.27004

10. Duan S, Xu C, Deng G, Wang J, Liu F, Xin SX. Quantitative analysis of the reconstruction errors of the currently popular algorithm of magnetic resonance electrical property tomography at the interfaces of adjacent tissues. *NMR Biomed.* 2016;29:744-750. doi:10.1002/nbm.3522

11. Hafalir FS, Oran OF, Gurler N, Ider YZ. Convection-reaction equation based magnetic resonance electrical properties tomography (cr-MREPT). *IEEE Trans Med Imaging.* 2014;33:777-793. doi:10.1109/TMI.2013.2296715

12. Park JE, Kim HS, Kim N, et al. Low conductivity on electrical properties tomography demonstrates unique tumor habitats indicating progression in glioblastoma. *Eur Radiol.* 2021;31:6655-6665. doi:10.1007/s00330-021-08065-8

13. Karsa A, Shmueli K. New approaches for simultaneous noise suppression and edge preservation to achieve accurate quantitative conductivity mapping in noisy images. In: *Proceedings of the 30th Annual Meeting of ISMRM [Virtual]*; 2021: Abstract 3774.

14. Balidemaj E, van den Berg CAT, Trinks J, et al. CSI-EPT: a contrast source inversion approach for improved MRI-based electric properties tomography. *IEEE Trans Med Imaging.* 2015;34:1788-1796. doi:10.1109/TMI.2015.2404944

15. Serralles JEC, Giannakopoulos II, Zhang B, et al. Non invasive estimation of electrical properties from magnetic resonance measurements via global Maxwell tomography and match regularization. *IEEE Trans on Biomed Eng.* 2019;67:3-15. doi:10.1109/TBME.2019.2907442

16. Mandija S, Meliadò EF, Huttinga NRF, Luijten PR, Berg CAT. Opening a new window on MR-based electrical properties tomography with deep learning. *Sci Rep.* 2019;9:1-9. doi:10.1038/s41598-019-45382-x

17. Hampe N, Katscher U, van den Berg CAT, Tha KK, Mandija S. Deep learning brain conductivity mapping using a patch-based 3D U-net. *arXiv preprint*: 1908.04118 2019.

18. Leijsen R, van den Berg CAT, Webb A, Remis R, Mandija S. Combining deep learning and 3D contrast source inversion in MR-based electrical properties tomography. *NMR Biomed.* 2022;35:e4211. doi:10.1002/nbm.4211

19. Wilkinson MD, Dumontier M, Aalbersberg IJJ, et al. The FAIR guiding principles for scientific data management and stewardship. *Sci Data.* 2016;3:160018. doi:10.1038/sdata.2016.18

20. de Buck MH, Jezzard P, Jeong H, Hess AT. An investigation into the minimum number of tissue groups required for 7T in-silico parallel transmit electromagnetic safety simulations in the human head. *Magn Reson Med.* 2021;85:1114-1122. doi:10.1002/mrm.28467

21. Cocosco CA, Kollokian V, Kwan RK-S, Pike G, Evans AC. *Brainweb: online interface to a 3D MRI simulated brain database.* CiteSeerX; 1997.

22. Fedorov A, Beichel R, Kalpathy-Cramer J, et al. 3D slicer as an image computing platform for the quantitative imaging network. *J Magn Reson Imaging.* 2012;30:1323-1341. doi:10.1016/j.mri.2012.05.001

23. Menze BH, Jakab A, Bauer S, et al. The multimodal brain tumor image segmentation benchmark (BRATS). *IEEE Trans Med Imaging.* 2014;34:1993-2024. doi:10.1109/TMI.2014.237769424

24. Bakas S, Reyes M, Jakab A, et al. Identifying the best machine learning algorithms for brain tumor segmentation, progression assessment, and overall survival prediction in the BRATS challenge. *arXiv.* 2018;(v3):1811.02629. doi:10.48550/arXiv.1811.02629

25. Christ A, Kainz W, Hahn EG, et al. The virtual family—development of surface-based anatomical models of two adults and two children for dosimetric simulations. *Phys Med Biol.* 2009;55:N23-N38. doi:10.1088/0031-9155/55/2/N01

26. Gabriel C. *Compilation of the Dielectric Properties of Body Tissues at RF and Microwave Frequencies.* Dept. of Physics; 1996.

27. Hancu I, Liu J, Hua Y, Lee SK. Electrical properties tomography: available contrast and reconstruction capabilities. *Magn Reson Med.* 2019;81:803-810. doi:10.1002/mrm.27453

28. Huhndorf M, Stehning C, Rohr A, et al. Systematic Brain Tumor Conductivity Study with Optimized EPT. In: *Proceedings of the 21st Annual Meeting of ISMRM*, Salt Lake City, Utah, USA. 2013.

29. Lu Y, Li B, Xu J, Yu J. Dielectric properties of human glioma and surrounding tissue. *Int J Hyperthermia.* 2019;8:755-760. doi:10.3109/0265673920900502330

30. Stijnman PR, Steensma BR, Van den Berg CAT, Raaijmakers AJ. A perturbation approach for ultrafast calculation of RF field enhancements near medical implants in MRI. *Sci Rep.* 2022;12:4224. doi:10.1038/s41598-022-08004-7

31. van Lier AL, Raaijmakers A, Voigt T, et al. Electrical properties tomography in the human brain at 1.5, 3, and 7T: a comparison study. *Magn Reson Med.* 2014;71:354-363. doi:10.1002/mrm.24637

32. Mandija S, Petrov PI, Vink JJ, Neggers SF, van den Berg CA. Brain tissue conductivity measurements with MR-electrical properties tomography: an in vivo study. *Brain Topogr.* 2021;34:56-63. doi:10.1007/s10548-020-00813-133

33. Crosas M. The dataverse network®: an open-source application for sharing, discovering and preserving data. *D-Lib Magazine.* 2011;17:1/2.

34. Jung KJ, Mandija S, Kim JH, et al. Improving phase-based conductivity reconstruction by means of deep learning–based denoising of phase data for 3T MRI. *Magn Reson Med.* 2021;86:2084-2094. doi:10.1002/mrm.28826

35. Mandija S, van den Berg CAT. The first MR electrical properties tomography (MR-EPT) reconstruction challenge. In: *Proceedings of the 31st Annual Meeting of ISMRM, London*; 2022: Abstract #704.

36. Arduino A. EPTlib: an open-source extensible collection of electric properties tomography techniques. *Appl Sci.* 2021;11:3237. doi:10.3390/app11073237

SUPPORTING INFORMATION

Additional supporting information may be found in the online version of the article at the publisher's website.

Data S1. Comparison of measurements and simulations on a cylindrical phantom.

Figure S1. Comparison of simulated and measured data for a cylinder phantoms. The top row shows the transceive

phase and $|B_1^+|$ along the anterior–posterior (AP) and left–right (LR) direction for simulation (dashed lines) and measurement (normal lines). On the bottom row, the first two images show conductivity reconstructions of the simulation and measurement in the center slice. The mean conductivity is indicated in red. The bottom right shows the distribution of the reconstructed conductivity.